Chemical Engineering Journal 452 (2023) 139399

Contents lists available at ScienceDirect

Chemical Engineering Journal

journal homepage: www.elsevier.com/locate/cej

Adsorption of emerging pollutants on lignin-based activated carbon: Analysis of adsorption mechanism via characterization, kinetics and equilibrium studies

L. Sellaoui [a,*], A. Gómez-Avilés [b], F. Dhaouadi [a], J. Bedia [b], A. Bonilla-Petriciolet [c], S. Rtimi [d], C. Belver [b,*]

[a] Laboratory of Quantum and Statistical Physics, LR18ES18, Monastir University, Faculty of Sciences of Monastir, Tunisia
[b] Chemical Engineering Department, Universidad Autónoma de Madrid, Campus Cantoblanco, E-28049 Madrid, Spain
[c] Instituto Tecnológico de Aguascalientes, Aguascalientes 20256, Mexico
[d] Global Institute for Water, Environment and Health, 1201 Geneva, Switzerland

ARTICLE INFO

Keywords:
Acetaminophen
Acetamiprid
Activated carbon
Adsorption

ABSTRACT

Lignin has been employed as a precursor to synthesize activated carbons with the aim of lignin-biomass revalorization. The properties of these activated carbons were compared, and the best adsorbent was employed to remove two emerging pollutants from water, acetaminophen and acetamiprid. The adsorption mechanisms of pharmaceutical and pesticide compounds were analyzed, modeled and interpreted via statistical physics models. In particular, adsorption kinetics and isotherms of acetaminophen and acetamiprid at temperatures between 20 and 60 °C were quantified experimentally. Equilibrium data were fitted to different statistical physics-based isotherm models to establish the corresponding adsorption mechanism. A double layer adsorption model with one type of functional group was the best to correlate and explain the removal of these organic molecules. Steric parameters for the adsorption of these organic compounds were also calculated thus determining that their adsorption was multi-molecular. At tested operating conditions, acetaminophen adsorption was endothermic, while acetamiprid removal was exothermic. Physical adsorption forces were expected to be responsible for the removal of both compounds. This study reports new insights on the adsorption mechanisms of relevant emerging pollutants commonly found in water worldwide.

1. Introduction

Pharmaceutical compounds and pesticides play a relevant role in health protection and agricultural activities [1,2]. Pharmaceuticals are relevant for medicine and disease prevention and are consumed worldwide [2], while pesticides are applied to control crop-damaging pests and disease vectors [1]. In terms of water treatment, these organic compounds are considered emerging pollutants [3–6]. The manufacturing of pharmaceuticals and their human consumption cause their subsequent entry into aquatic ecosystems [7]. In the case of pesticides, their presence in the environment has a common origin in agricultural activities and reaches water bodies after being dissolved and transported mainly by stormwater runoff [8]. Some studies have indicated that these emerging organic pollutants can be still identified in the effluents obtained from traditional wastewater treatment because they are not completely removed and, consequently, their persistence generates environmental pollution that could imply a negative effect on the ecosystems [9,10]. The use of activated carbon (AC) for water treatment offers the possibility to remove different organic and inorganic pollutants through adsorption, which can be tailored via the incorporation of specific functional groups on the adsorbent surface to enhance the removal of the target molecules. For instance, this adsorbent has been widely employed to study the adsorption of textile pollutants [11–15], pesticides [16,17], heavy metals [18,19], and pharmaceuticals [20]. Numerous studies describing the removal of organic compounds via the AC-based adsorption process showed that it has a good performance and is attractive for several industrial applications to reduce water pollutant concentrations [21].

ACs are amorphous materials commonly prepared from different carbon precursors [22], with special attention being given to the use of

* Corresponding authors.
E-mail addresses: sellaouilotfi@yahoo.fr (L. Sellaoui), carolina.belver@uam.es (C. Belver).

https://doi.org/10.1016/j.cej.2022.139399
Received 27 July 2022; Received in revised form 19 September 2022; Accepted 20 September 2022
Available online 23 September 2022

biomass wastes, aimed at their revalorization and the reduction of the carbon footprint. Two different ways allow the preparation of AC from carbon precursors, named chemical and physical activations [22]. During the chemical activation, the carbon precursor is first impregnated with an activating agent (H_3PO_4, $ZnCl_2$, $FeCl_3$, among others), then the mixture is subjected to thermal treatment or pyrolysis and finished with a washing. When the physical activation is used, the carbon precursor is subjected to two thermal stages. The activation starts with pyrolysis at a high temperature in an inert atmosphere and ends with gasification using an agent (CO_2, O_2, among others). In our study, several ACs were prepared from lignin, a known waste from pulp and paper industries and fuel plants, which revalorization is currently under study [23,24]. Chemical activation was selected as the synthesis route using $FeCl_3$ as an activating agent, which efficiency has been studied before regarding the textural parameters developed by the ACs [22,25–27]. A complete screening of the activation conditions was performed, aiming to the generation of an AC with tailored properties for water treatment by adsorption. Regarding the removal of emerging pollutants, acetaminophen and acetamiprid were selected to evaluate the adsorption capacity of the AC. In particular, acetaminophen is an analgesic and is one of the most known pharmaceutical pollutants due to its presence in surface and potable water [28,29]. Concerning acetamiprid, it is a neonicotinoid insecticide included in the *first watch list under the environmental quality standards* developed by the European Commission [30]. Some studies showed that its concentrations in water samples could vary from 0.008 to 44.1 $\mu g \cdot L^{-1}$ [31]. Therefore, the removal of both organic pollutants is necessary to reduce environmental pollution [31].

In this paper, statistical physic-based models were applied to understand the removal of these emerging organic pollutants. Different scenarios for the adsorption mechanism were proposed to analyze the removal of these compounds. It was assumed that the adsorption of tested adsorbates implied a monolayer adsorption process via the interaction with one or two types of surface functional groups and a double layer process. The main objective of this paper was to establish the adsorption mechanism of these organic pollutants via statistical physics models to provide a non-classical understanding in terms of the estimation of the total number of adsorbed pollutant layers and the number of pollutant molecules that can be adsorbed by AC functional group(s) besides the corresponding adsorption energies. These steric parameters were employed to describe the AC performance.

2. Experimental section

2.1. Materials

Lignin alkali in powder, iron (III) chloride hexahydrate ($FeCl_3 \cdot 6H_2O$, ACS reagent, 97 %), HCl (ACS reagent, 37 %), acetic acid (purity ≥ 99 %), acetaminophen (ACE; ≥99 %) and acetamiprid (ACTMPD; ≥98 %) were procured from Sigma Aldrich. Acetonitrile (HPLC grade) was purchased at Scharlab and used as a mobile phase for liquid chromatography.

Table 1
Elemental composition, ash proportion and yields (dry basis).

	%C	%H	%N	%O*	Ash (%)	Yield (%)
Lignin	61.6	6.0	1.1	29.3	2.0	–
R1-500	81.5	2.6	0.4	9.2	6.3	47.1
R1-700	85.0	1.4	0.2	9.2	4.2	42.1
R1-900	86.2	0.8	0.3	5.0	7.7	38.7
***R*3-500**	85.3	2.4	0.3	10.5	1.5	41.8
***R*3-700**	87.8	1.2	0.3	6.3	4.4	36.0
***R*3-900**	88.1	0.7	0.3	2.9	8.0	26.3
R5-500	84.4	2.3	0.3	11.6	1.4	37.4
R5-700	86.0	1.2	0.3	8.8	3.7	34.8
R5-900	87.1	0.7	0.3	2.5	9.4	19.9

* calculated by difference.

2.2. Preparation of the activated carbons

Lignin (5 g) was physically mixed with $FeCl_3 \cdot 6H_2O$ at different mass ratios (g $FeCl_3$/g lignin on a dry basis, values from 1 to 5). The mixture was homogenized by grinding, transferred to a ceramic crucible, and put in an oven at 60 °C for 24 h. Then, it was placed in a tubular muffle by passing a stream of N_2 (100 $mL \cdot min^{-1}$) to guarantee an inert atmosphere inside. The activation was performed at three different temperatures (500, 700, and 900 °C) for 2 h, maintaining the nitrogen flow during the cooling down. The resulting carbon samples were washed with an aqueous HCl (1 M) solution at 70 °C for 2 h and then rinsed with distilled water at room temperature up to neutral pH of the eluate. Finally, the samples were dried overnight in an oven at 60 °C. The resulting AC samples were denoted as RX-T, being X the impregnation ratio and T the heating temperature (e.g., R1-500 is the AC obtained with an impregnation ratio of 1 and activated at 500 °C).

2.3. Characterization techniques

Elemental analyses were performed using a LECO CHNS-932 analyzer to quantify the C, N and H contents of the AC samples. The porous texture was characterized by N_2 adsorption–desorption at –196 °C using a Micromeritics Tri Star II apparatus. Before the analysis, the samples (around 150 mg) were outgassed at 150 °C overnight to clean the surface. Brunauer-Emmett-Teller (BET) method was used to calculate the BET surface area (S_{BET}) [32], while the micropore volume (V_{micro}) and the non-microporous or so-called external area (S_{EXT}) were calculated by the *t*-plot method [33]. The total volume of pores (V_{pore}) was estimated from the amount (expressed as liquid) of N_2 adsorbed at 0.99 relative pressure. The AC sample with the most developed porous texture was subjected to further characterization. The pH drift method was used to obtain the pH at the point of zero charge (pH_{PZC}) [34]. For that purpose, 50 mL of NaCl solution (0.01 M) were placed in a closed titration vessel. The pH value was adjusted from 1 to 13 using HCl (0.1 M) or NaOH (0.1 M) aqueous solutions. 20 mg of AC were suspended in the different solutions and bubbled with N_2 for 2 min to remove dissolved gasses. After 24 h under stirring, the pH was measured and plotted versus the initial one, the intersection of both curves corresponds to the pHpzc. Fourier Transform Infrared (FTIR) spectra were recorded in a Brukeri FS 66VS spectrometer in the wave number range of 4000–400 cm^{-1} with a 2 cm^{-1} resolution. The samples were mixed with KBr and pelletized before the analysis. The morphology of the AC before and after adsorption was studied by scanning electron microscopy (SEM, Hitachi S4800) at an accelerating voltage of 15 kV using secondary electron (SE) and backscattered electron (BSE) detectors.

2.4. Liquid-phase adsorption experiments

The adsorption experiments were performed by adding 40 $mg \cdot L^{-1}$ of AC to a solution (250 mL) of ACE or ACTMPD at different initial concentrations (5, 10, 20, 40, 60, 80, and 100 $mg \cdot L^{-1}$). The suspensions were stirred at 200 rpm for 24 h at different adsorption temperatures (20, 40, and 60 °C) in a water bath orbital shaker. After adsorption time, 1 mL of the aqueous solution was sampled and filtered with a PTFE syringe filter (Whatman 0.45 μm). Kinetic adsorption tests were also performed in the same way with an initial pollutant concentration of 20 $mg \cdot L^{-1}$, sampling at different time intervals. ACE and ACTMPD adsorption of R5-900 were evaluated upon three consecutive cycles. After each cycle, the material was filtered, washed with stirring distilled water at 90 °C for 2 h, and dried at 60 °C overnight, ensuring that the adsorption conditions among cycles were similar. The ACE and ACTMPD concentrations in the liquid phase were quantified by liquid chromatography using a Shimadzu Prominence-I LC-2030C chromatograph (HPLC), equipped with a diode array detector (SPDM30A) and a C18

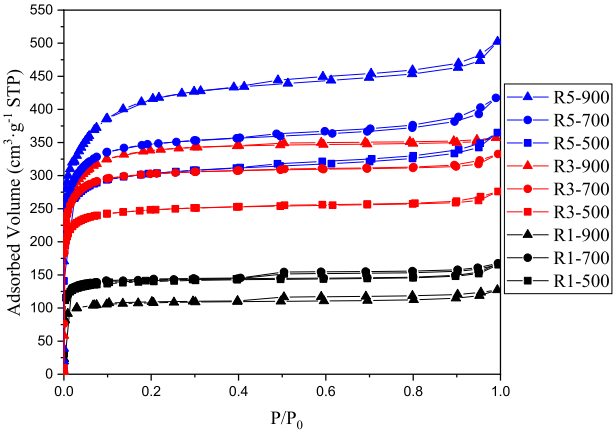

Fig. 1. N_2 adsorption–desorption isotherms at −196 °C of all ACs.

Table 2
Summary of the porous texture of the ACs.

	S_{BET} ($m^2 \cdot g^{-1}$)	S_{EXT} ($m^2 \cdot g^{-1}$)	S_{micro} ($m^2 \cdot g^{-1}$)	V_{micro} ($cm^3 \cdot g^{-1}$)	V_{pore} ($cm^3 \cdot g^{-1}$)
R1-500	453	53	400	0.19	0.26
R1-700	460	40	420	0.20	0.26
R1-900	345	36	309	0.15	0.20
***R*3-500**	829	102	727	0.35	0.45
***R*3-700**	899	90	809	0.44	0.53
***R*3-900**	1090	189	901	0.44	0.55
R5-500	975	129	846	0.43	0.58
R5-700	1127	189	938	0.45	0.65
R5-900	1469	448	1022	0.49	0.82

* S_{BET}, specific surface area; S_{EXT}, external surface area; S_{micro}, micropore surface area; V_{micro}, micropore volume; V_{pore}, total pore volume.

column (ZORBAX Eclipse Plus 5 µm, Agilent). The mobile phase was a mixture of acetonitrile/acetic acid (0.1 v/v%). The ACE detection required a gradient method (from 10/90 to 40/60 %) with a flow rate of 0.7 mL·min^{-1}and a wavelength set at 246 nm, while an isocratic method (22/78 %) was used for the ACTMPD quantification with a 0.8 mL·min^{-1} flow rate and a wavelength fixed at 244 nm.

3. Results and discussions

3.1. Characterization of the activated carbons

Table 1 summarizes the elemental analyses and ash content of raw lignin and the resulting ACs, with the corresponding yield values (i.e., AC to lignin mass percentage on a dry basis). Deep carbonization takes place in all cases, being similar carbon percentages. Lower H content was observed by increasing the temperature from 500 to 900 °C. The high ash content of samples obtained with activation temperatures of 900 °C may be associated with the presence of residual iron compounds strongly attached to the carbon surface that remains after the washing step and to the deeper devolatilization achieved at this high activation temperature (in agreement with the lower yields).

Fig. 1 shows the N_2 adsorption–desorption isotherms at –196 °C of all ACs prepared, and Table 2 collects the main features relative to the porous texture. All ACs showed isotherms characteristic of microporous solids, with remarkable N_2 adsorption at low relative pressures, with a minor contribution of mesoporosity [35] as confirmed by the low values of the S_{EXT} and the high V_{micro} values. Regarding the impregnation ratio, it is clear its influence on the textural parameters. Higher loads of the activating agent (R5 series) resulted in better development of the porosity due to the chemical interaction of the iron precursor with the lignin surface. The temperature of the thermal treatment is also a key parameter. The porosity development enhances with increasing temperature, except for the series R1 where the development is very similar at 500 and 700 °C, and even lower for 900 °C, maybe due to a partial contraction of the porous structure at this high activation temperature [34]. The conditions resulting in the highest porosity development were an activation temperature of 900 °C with the highest impregnation ratio (R5). These conditions resulted in an AC with a high surface area, close to 1500 $m^2 \cdot g^{-1}$, higher than those reported for the chemical activation of lignin with $FeCl_3$ by microwave heating [34] and from other precursors also with $FeCl_3$ by conventional heating [27], and close to the obtained by chemical activation of Tara gum with the same activating agent (1600 $m^2 \cdot g^{-1}$) [36]. The activation with other activating agents (e.g. H_3PO_4) would lead to activated carbons with a higher amount of mesoporosity. However, this does not always result in better adsorption, even in a liquid phase. Regardless of this, the activated carbon with the most developed porosity, R5-900, which was selected for the subsequent adsorption tests, has a micropore volume of 0.49 $cm^3 \cdot g^{-1}$ and a mesopore volume of 0.33 $cm^3 \cdot g^{-1}$. That is to say, the mesopore ratio is around 40 % (percentage of mesopores relative to the total pore volume), which can be considered a very significant proportion of mesoporosity. Thus, the R5-900 AC herein prepared appears as a promising adsorbent thanks to its remarkable porosity and, consequently, it was selected for further characterization.

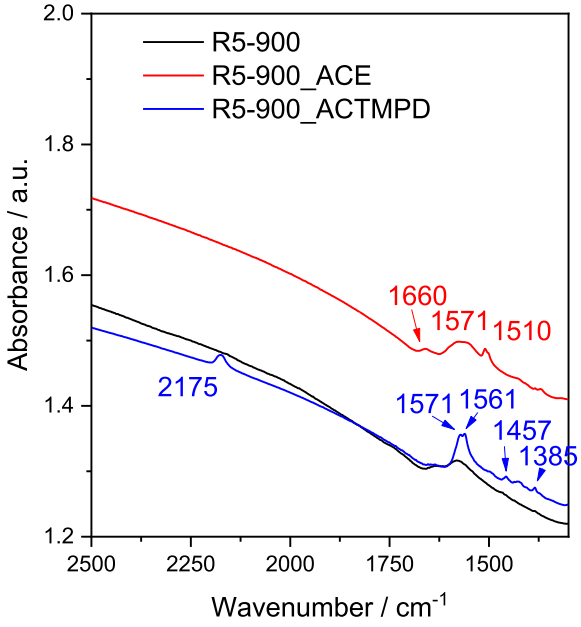

Fig. 2. FTIR spectra of R5-900 AC before and after ACTMPD and ACE adsorption.

The pH_{PZC} value of the R5-900 was established at 6.3. This means that at higher pH its surface remains negatively charged, while it is positively charged at pH lower than 6.3 [37]. ACE is a weak acid (pK_a = 9.38) that is neutrally charged at pH below 9.3, while ACTMPD is a strong acid (pK_a = 0.7) appearing mostly in its negative form. Because of this large difference, the adsorption experiments were performed at natural pH (i.e.: 6.6 and 6.1 for ACE and ACTMPD, respectively). At these pH values, the R5-900 surface was neutrally charged, while the ACE molecule remained uncharged and the ACTMP molecule was positively charged. Thus, since both target pollutants were successfully adsorbed, the adsorption was not controlled by the electrostatic interaction, as has been already reported in the literature [34,38,39].

Fig. 2 compares the FTIR spectra of the R5-900 adsorbent before and after the adsorption of both pollutants. ACTMPD adsorption generated the identification of new absorption bands at 2500–1250 cm^{-1} range.

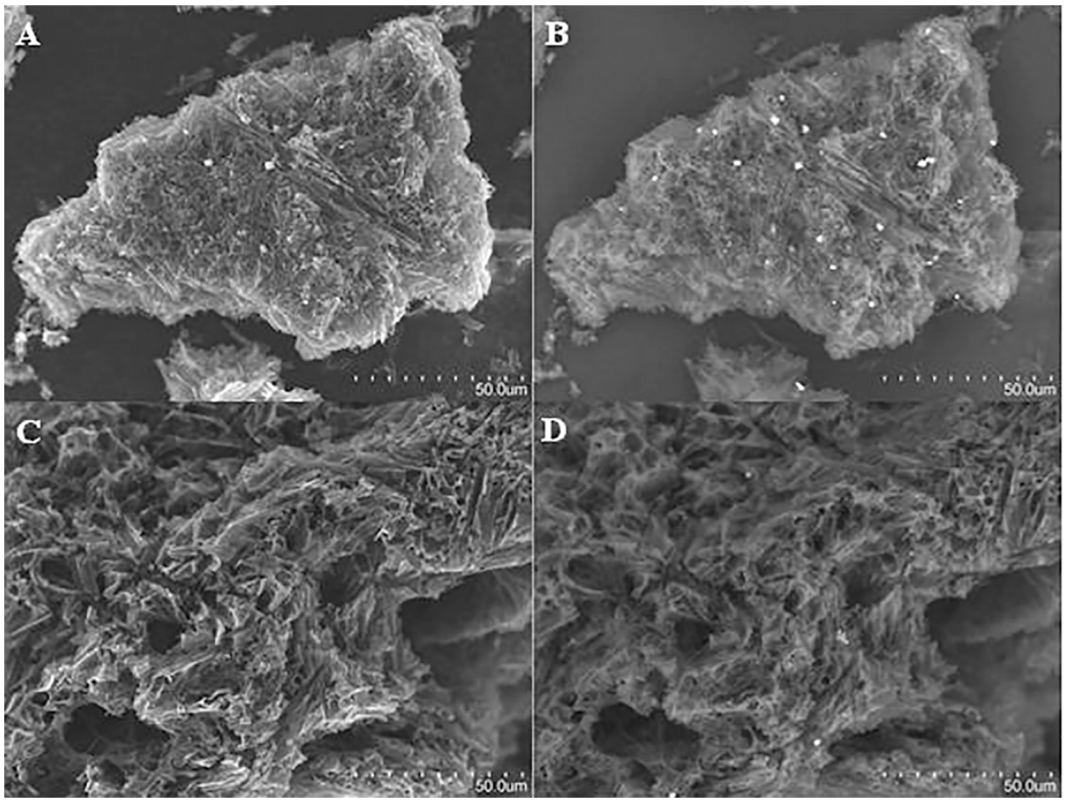

Fig. 3. SEM images of the R5-900 AC before and after adsorption using secondary electron (A and C, respectively) and backscattered electron (B and D, respectively) detectors.

The bands of –C—N and –C═N stretching vibrations appear at 2175 and 1561 cm^{-1}, respectively, while the absorption band of –C═C– vibration of the aromatic ring can be seen at 1571 cm^{-1} [40]. The olefinic = CH– groups of the pyridine group can be identified with the 1457 cm^{-1} band, and the –C—N stretching vibrations can be associated with the band at 1381 cm^{-1} [41]. The ACE adsorption at the AC surface yielded new absorption bands in the FTIR spectrum of the R5-900. The bands of –C═O–N stretching and –C—N—H bending vibrations appear at 1660 and 1571 cm^{-1}, respectively. The band associated with the stretching vibrations of –CNC = O is located at 1510 cm^{-1} [42]. SEM characterization of R5-900 after adsorption was also performed, Fig. 3 shows the images using secondary electron (SE) and backscattered electron (BSE) detectors. The R5-900 sample is characterized by a very non-uniform surface, covered by tunnels and voids with thin walls distributed throughout the solid, generated by the loss of volatile organic matter during the activation process (Fig. 3A and B). The presence of small crystals is evident in R5-900, mostly in the BSE image in Fig. 3B, which was associated with the crystallization of iron oxide not removed during the washing stage, in agreement with a previous study [27]. These morphological characteristics remain unchanged after adsorption (as can be observed by comparing SEM images in Fig. 3), indicating the stability of the AC during the adsorption process.

3.2. A general description of the modeling strategy of organic molecules adsorption on AC

The adsorption kinetics of ACTMPD and ACE is reported in Fig. 4. These experimental data showed that the adsorption temperature caused a different effect on the removal of these compounds. A reduction in the adsorbed quantity of ACTMPD was observed as the solution temperature increased, while the adsorption capacity of the ACE molecule decreased with the adsorption temperature. In terms of adsorption kinetics, the removal of these pollutants was fast and reached the adsorption equilibrium after less than 250 min (Fig. 4). We fitted the experimental data two the most common kinetic models, pseudo-first order and pseudo-second order. Table 3 reports the models' equations besides the characteristic parameters obtained by non-linear fitting and the determination coefficients. The pseudo-second order model (R^2 = 0.98 – 0.99) outperformed the pseudo-first order model (R^2 = 0.95 – 0.99) to fit the kinetics of adsorption of both ACE and ACTMPD. Calculated adsorption rate constants (k_{p2}) ranged from 0.00033 to 0.00049 $g{\cdot}mg^{-1}{\cdot}min^{-1}$ for ACE and from 0.00033 to 0.00038 $g{\cdot}mg^{-1}{\cdot}min^{-1}$ for ACTMPD. The adsorption rate constants of ACE were higher than those of ACTMPD molecule suggesting its faster adsorption. There is a significant difference in the molecular dimensions of these compounds and, consequently, it could be expected that ACE (i.e., the smallest molecule) would show a faster mass transfer than that of ACTMPD (i.e., the largest molecule). Overall, the adsorption rate constants of ACE increased with the adsorption temperature, while the values of k_{p2} for ACTMPD decreased with the adsorption temperature. These trends indicated the existence of endothermic adsorption for ACE and exothermic adsorption for ACTMPD.

Fig. 5 depicts the experimental adsorption isotherms of ACTMPD and ACE performed at initial concentrations from 20 to 100 $mg{\cdot}L^{-1}$. Adsorption tests at three temperatures (20, 40 and 60 °C) were also performed at a low initial concentration, 1 $mg{\cdot}L^{-1}$. In all cases (six tests), the concentration of the pollutant was zero (or at least below the HPLC sensitivity). So, it seems that the synthesized carbons could be used even for the treatment of streams with very low pollutant concentrations, although to further confirm this assumption dynamic adsorption tests should be performed. All isotherms corresponded to the typical L-type form in the liquid phase [43], where the adsorption capacities of both organic pollutants increased as a function of the equilibrium concentration up to a maximum value to reach a saturation plateau thus implying that the active sites accessible on the R5-900 surface are expected to be filled by the pollutant molecules. This phenomenon also

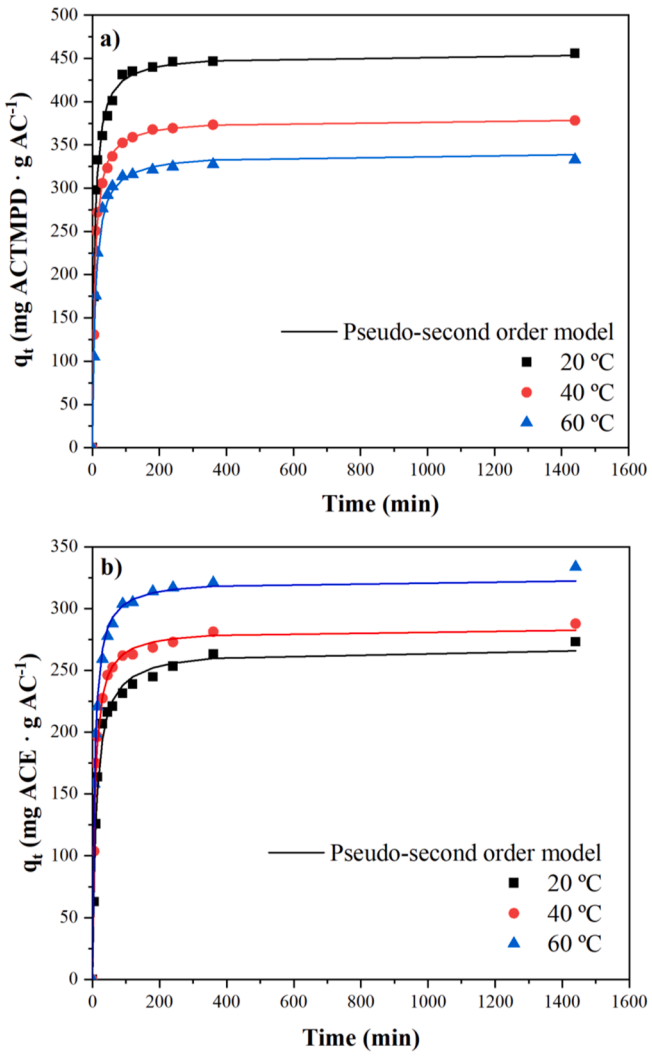

Fig. 4. Kinetics of the adsorption of ACTMPD (a) and ACE (b) on R5-900 AC at 20 – 60 °C and pH 6.6 and 6.1, respectively. Experimental conditions: $[ACE]_0$ = 20 mg·L^{-1}; $[ACTMPD]_0$ = 20 mg·L^{-1}; V = 250 mL; [adsorbent] = 40 mg·L^{-1}.

implied the formation of a fixed number of adsorbate layers on the R5-900 surface.

Three adsorption models developed by statistical physics were applied to fit all the isotherms and determine the number of layers formed by these organic molecules on the adsorbent surface and elucidate the adsorption mechanism at the molecular scale. These models are described below, the expressions for the adsorbed quantities and adsorption energies associated with these models are summarized in Table 4, which can attribute in general new findings of the adsorption mechanism contrary to classical models:

Model 1: This model assumed that organic pollutant molecules were arranged to form a monolayer on the R5-900 surface involving the interaction with only one type of functionality where one interaction energy characterized the adsorption process. Note that each functionality from the R5-900 surface can adsorb a variable number of pollutant molecules [44,45], which was contrary to the theory supporting the most known adsorption models reported in the literature (e.g., the Langmuir model).

Model 2: This model supposed that the adsorption mechanism was carried out on two types of active sites from the R5-900 surface where their contributions were different. These two types of functionalities can adsorb several pollutant molecules and they can form a single adsorbed pollutant layer [44,45].

Model 3: These organic compounds could form two layers on the R5-900 surface where two interaction energies were involved. One energy described the interactions between the R5-900 surface functionalities and the pollutant molecules, and the other energy characterized the interactions between the adsorbate molecules [46].

These models were tested on the experimental equilibrium data using a multivariable nonlinear regression with the Levenberg-Marquardt algorithm. The selection of the best adsorption model was mainly based on the determination coefficient R^2 (which is illustrated in Table 5) and the suitable trend of the model parameters as a function of adsorption temperature. The corresponding physicochemical parameters are given in Table 6 and the isotherms fitted by this model are shown in Fig. 5. Model 3 (double layer model) showed the highest determination coefficients (R^2 = 0.995–0.999) and outperformed other tested models. Also, the variation of their steric and energetic parameters as a function of the solution temperature was interpretable thus allowing to analyze the adsorption mechanism. Hence, this double-layer model was applied to explain the adsorption equilibrium of these organic molecules at tested operating conditions.

3.3. Investigation of organic molecules adsorption phenomenon via steric and energetic parameters

The evolution of the number of molecules adsorbed by R5-900 and their density with respect to the solution temperature is represented in Fig. 6. All values of n_m were above unity, which suggested that the adsorption mechanism of these target pollutants was multi-molecular where each active site of the R5-900 surface could adsorb several molecules simultaneously. The temperature had a favorable effect on the variation of the number of adsorbed pollutant molecules per R5-900 active site, hence the thermal agitation promoted the aggregation of the molecules in the solution and its degree could tend to form a dimer.

Table 3
Calculated kinetic parameters for the adsorption of ACE and ACTMPD molecules on R5-900 AC.

		Model ±					
		Pseudo-first order kinetic $Q_t = Q_{te}[1 - exp(k_{p1}t)]$			Pseudo-second order kinetic $Q_t = \frac{k_{p2}Q_{te}^2 t}{1 + k_{p2}Q_{te}t}$		
Compound	**T (°C)**	**k_{p1} (min^{-1})**	**q_{te} (mg·g^{-1})**	**R^2**	**k_{p2} (g·mg^{-1}·min^{-1})**	**q_{te} (mg·g^{-1})**	**R^2**
Acetaminophen	20	0.06	246.1	0.97	0.00033	267.9	0.98
	40	0.09	265.7	0.98	0.00049	283.9	0.99
	60	0.10	304.3	0.95	0.00049	323.7	0.99
Acetamiprid	20	0.10	426.9	0.96	0.00033	455.5	0.99
	40	0.09	355.9	0.97	0.00038	380.1	0.98
	60	0.07	317.9	0.99	0.00033	340.8	0.99

±Q_t is the molecule adsorption capacity (mg·g^{-1}) at time t (min), k_{p1} (min^{-1}) and k_{p2} (g·mg^{-1}·min^{-1}) are the adsorption rate constants of pseudo-first and pseudo-second orders, respectively, and q_{te} (mg·g^{-1}) is the theoretical equilibrium adsorption capacity.

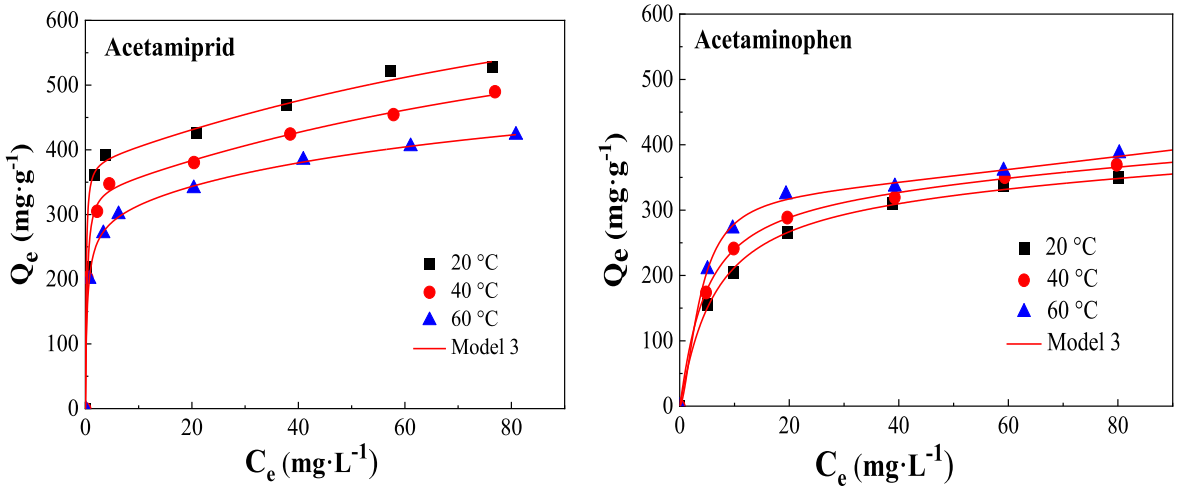

Fig. 5. Isotherms of ACTMPD and ACE adsorption on R5-900 at 20, 40 and 60 °C and pH 6.1 and 6.6, respectively.

Table 4
Analytical expressions used to estimate the adsorbed quantities and the adsorption energies [44–46]. Nomenclature: $C_{1/2}$ represents the concentration at half-saturation of the formed layer related to model 1; C_1 and C_2 are the concentrations at half-saturation associated with the two types of adsorption sites (model 2); C_1 and C_2 are also the concentrations at half-saturation associated to the first and second layer (model 3). In all expressions, C_s represent the water solubility of the investigated adsorbate.

	Model 1	Model 2	Model 3
Adsorption capacity Q_e	$\frac{n_m D_{as}}{1+\left(\frac{C_{1/2}}{C_e}\right)^{n_m}}$	$\frac{n_{m1} D_{as1}}{1+\left(\frac{C_1}{C_e}\right)^{n_{m1}}} + \frac{n_{m2} D_{as2}}{1+\left(\frac{C_2}{C_e}\right)^{n_{m2}}}$	$n_m D_{as} \frac{\left(\frac{C_e}{C_1}\right)^{n_m} + 2\left(\frac{C_e}{C_2}\right)^{2n_m}}{1+\left(\frac{C_e}{C_1}\right)^{n_m} + \left(\frac{C_e}{C_2}\right)^{2n_m}}$
Adsorption energy ΔE_i	$\Delta E = RT\ln\frac{C_s}{C_{1/2}}$	$\Delta E_{1,2} = RT\ln\frac{C_s}{C_{1,2}}$	$\Delta E_{1,2} = RT\ln\frac{C_s}{C_{1,2}}$

Table 5
Coefficient of determination R^2 associated with the three tested analytical models.

T (°C)	Model 1	Model 2	Model 3
Acetamiprid			
20	0.890	0.999	0.996
40	0.921	0.994	0.997
60	0.860	0.997	0.995
Acetaminophen			
20	0.999	0.999	0.998
40	0.997	0.999	0.999
60	0.991	0.998	0.997

One adsorption site of R5-900 was responsible to capture more than one pollutant molecule thus suggesting that these adsorbates were removed via an inclined position on the R5-900 surface. The variation of parameter D_{as} (Fig. 6) can be considered as a measure of the effect of thermal agitation on the number of active sites that participated in the removal mechanism of these molecules. The trend of this parameter showed that the solution temperature favored the reduction of the active site density for both compounds. Moreover, the endothermic behavior of the molecular aggregation phenomenon may lead to the reduction of free space on the R5-900 surface and, in consequence, there was a limitation occupying the active sites that remained available to interact with these organic molecules.

The interpretation of the adsorption capacity at saturation completes the understanding of the adsorption mechanism of these organic molecules and, also, describes the adsorbent performance. The values of this parameter are directly calculated by the next expression that assumed the formation of 2 adsorbate layers: $Q = 2{\cdot}n_m{\cdot}D_{as}$. The calculated values of saturation adsorption capacities of ACTMPD were higher than those of ACE at 20 and 40 °C, the ACE adsorption was higher than that of ACTMPD at 60 °C (i.e., 595.58 and 655.50 $mg{\cdot}g^{-1}$ for ACTMPD and ACE, respectively). It was expected that the removal of both compounds was via the same AC functional group. However, opposite thermodynamic behaviors were observed for the adsorption of these compounds with respect to the solution temperature. The first was related to the ACTMPD adsorption where a reduction in the adsorption capacity was observed with the temperature increment, while the second one showed that the ACE adsorption capacity increased slightly with the solution temperature (Fig. 7). These differences could be associated with the impact of adsorbate molecular dimensions on mass transfer during the adsorption process. In particular, the molecular dimensions and molecular weight of ACTMPD are higher than those of the ACE molecule. This implies that ACTMPD molecules can face steric restrictions to access the internal micropore structure of tested activated carbon. Besides as the adsorption temperature increased, the kinetic energy of these molecules increased especially for the compound with the lowest molecular mass thus favoring the interaction with the adsorbent active sites. Therefore, different thermodynamic behavior was observed for these pollutants.

It is noteworthy that R5-900 showed better adsorption capacities of ACE than those reported for other adsorbents, see Table 7. For instance, the removal of ACE has been studied using AC prepared from different sources, such as lignin, Pyrolyzed pulp mill sludge, Oak fruits biomass, and Rice Husk where their maximum adsorption capacities are listed in Table 7. This study showed that R5-900 was a promising adsorbent to treat the water containing these organic molecules. Note that its adsorption capacities to remove the ACE molecules varied from 647.5 to 655.5 $mg{\cdot}g^{-1}$. Besides, the recycling performance and stability of the R5-900 adsorbent were studied by 3-cycle tests for 24 h at 40 °C (Fig. 8). The removal of both ACE and ACTMPD targets show a similar trend, without important deviations in the adsorption capacity. This result proves the stability of the R5-900 adsorbent and its potential for cycling use applications.

The two half saturation concentrations obtained from the adsorption isotherm fitting were used to calculate the adsorption energies of two layers formed on the R5-900 surface according to the next mathematical relations [46]:

Table 6
Physicochemical parameters related to the adsorption mechanism of ACTMPD and ACE on R5-900. Nomenclature: n_m is the number of pollutant molecules adsorbed per R5-900 adsorption site, D_{as} is the active site density (mg·g^{-1}), C_i (mg·L^{-1}) is the concentration at half saturation, SE is the Standard error and Q_0 (mg·g^{-1}) is the adsorbed quantity at saturation.

T (°C)	n_m	SE	D_{as} (mg·g^{-1})	SE	C_1 (mg·L^{-1})	SE	C_2 (mg·L^{-1})	SE	Q_0 (mg·g^{-1})	SE
Acetamiprid										
20	1.13	0.0565	338.80	16.94	0.14	0.0183	4.04	0.498	765.68	38.284
40	1.17	0.0585	290.75	14.537	0.29	0.035	5.40	0.643	680.35	34.017
60	1.30	0.065	229.07	11.453	0.44	0.045	6.44	0.834	595.58	29.77
Acetaminophen										
20	1.08	0.054	299.77	14.98	5.92	0.20	53.37	0.468	647.50	32.375
40	1.12	0.056	290.23	14.511	4.30	0.256	39.02	2.0015	650.11	32.505
60	1.67	0.0835	196.26	9.813	3.68	0.09	27.73	3.046	655.50	32.775

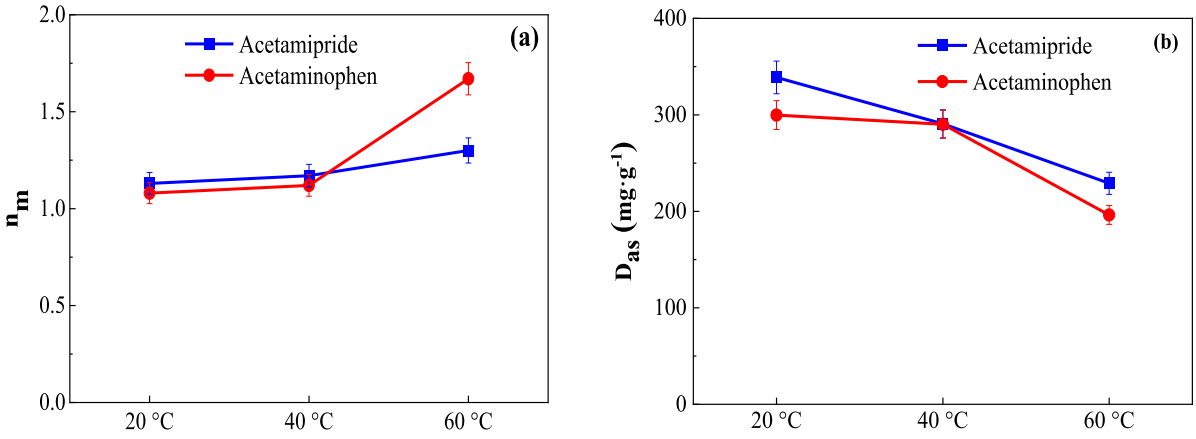

Fig. 6. Impact of the solution temperature on the number of ACTMPD and ACE molecules adsorbed per R5-900 active site (a) and their density (b).

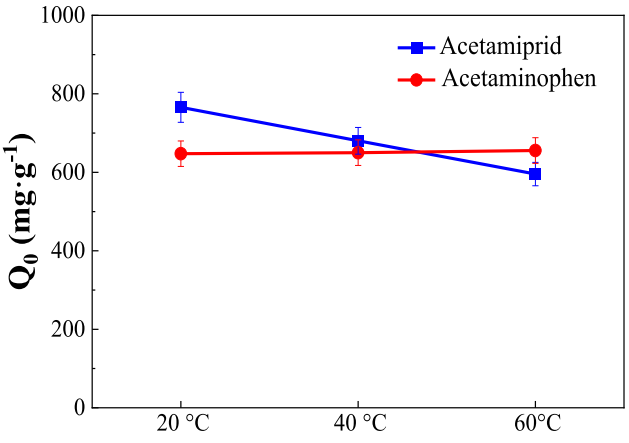

Fig. 7. Impact of solution temperature on the adsorption capacity at saturation for the removal of ACE and ACTMPD on R5-900.

$$\Delta E_1 = RT\ln\frac{C_s}{C_1}$$

$$\Delta E_2 = RT\ln\frac{C_s}{C_2}$$

where C_s is the water solubility (mg·g^{-1}) of the organic adsorbate molecules and $R = 8.314$ J·mol^{-1}·K^{-1} is the ideal gas constant. Table 8 reports the adsorption energies associated with the two formed layers that were calculated with the previous expressions. The calculated values of the adsorption energies of the target molecules on the R5-900 surface were below 40 kJ·mol^{-1}, thus indicating that only physical interactions were taking place in the removal of these molecules. It was found that: $\Delta E_1 > \Delta E_2$. This outcome can be explained as a logical consequence of the fact that the first adsorption energy was related to the direct binding of the target molecules with the AC surface.

4. Conclusions

Activated carbons were prepared from lignin by chemical activation with $FeCl_3$ with a well-developed microporosity. By setting the optimum conditions for the activation, a high porous activated carbon was obtained with a high specific surface area (1500 m^2·g^{-1}). This activated

Table 7
Comparison of the AC performance and other adsorbents available in the literature for ACE removal.

Adsorbent	Q_{max} ($mg \cdot g^{-1}$)	S_{BET} ($m^2 \cdot g^{-1}$)	Parameters	Reference
R5-900	655.5	1469	$[ACE]_0$ = 10–100 $mg \cdot L^{-1}$ [Adsorbent] = 0.25 $g \cdot L^{-1}$	This work
Lignin activated carbon	300	1177	$[ACE]_0$ = 10–100 $mg \cdot L^{-1}$ [Adsorbent] = 0.25 $g \cdot L^{-1}$	[34]
Biomass-derived activated carbon	100	990	$[ACE]_0$ = 0–20 $mg \cdot L^{-1}$ [Adsorbent] = 0.1 $g \cdot L^{-1}$	[47]
Organo-sepiolite	67.7	83	$[ACE]_0$ = 10–100 $mg \cdot L^{-1}$ [Adsorbent] = 0.25 $g \cdot L^{-1}$	[48]
Oak fruits	58.7	298	$[ACE]_0$ = 5–150 $mg \cdot L^{-1}$ [Adsorbent] = 1 $g \cdot L^{-1}$	[38]
MCM-41-graphene	322.6	327	$[ACE]_0$ = 25–200 $mg \cdot L^{-1}$ [Adsorbent] = 0.75 $g \cdot L^{-1}$	[49]
Activated carbon prepared from Rice Husk	21	178	$[ACE]_0$ = 70–120 $mg \cdot L^{-1}$ [Adsorbent] = 5 $g \cdot L^{-1}$	[50]
Pyrolyzed pulp mill sludge	19.7	209	$[ACE]_0$ = 100 $mg \cdot L^{-1}$ [Adsorbent] = not provided	[51]

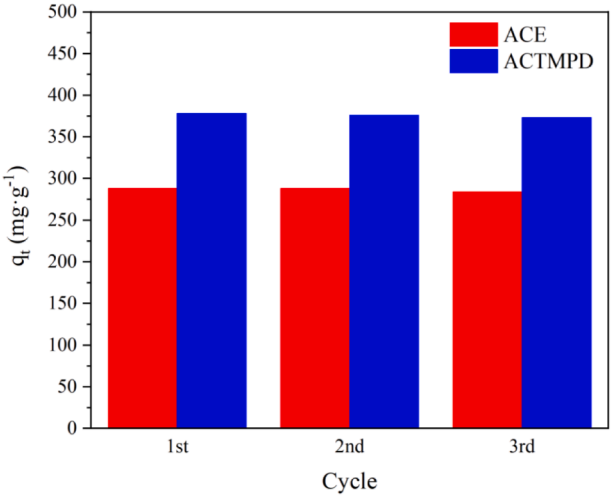

Fig. 8. ACE and ACTMPD adsorption after three consecutive cycles with R5-900 after 24 h at 40 °C ($[ACE]_0$, $[ACTMPD]_0$ = 20 $mg \cdot L^{-1}$).

carbon was tested for the removal of emerging pollutants present in water, named acetamiprid and acetaminophen. The adsorption mechanisms were studied via statistical physics theory. Results showed that the adsorption of these organic compounds was multimolecular where molecular aggregates could be formed. Two layers can be produced in the adsorption of these emerging pollutants on the activated carbon surface. Acetaminophen adsorption was endothermic, while acetamiprid adsorption was exothermic on tested activated carbon. This adsorption behavior could be associated with the molecular dimension of these adsorbates, which affected the mass transfer phenomena. However, this lignin-based activated carbon showed the best adsorption capacities for the removal of acetamiprid, especially at low adsorption temperatures. This study provides new insights on the adsorption of pharmaceutical and pesticide molecules on activated carbon to consolidate its application in water treatment.

Table 8
Calculated ΔE_1 and ΔE_2 as a function of solution temperature for the adsorption of ACTMPD and ACE on R5-900.

T(°C)	ΔE_1 ($kJ \cdot mol^{-1}$)	ΔE_2 ($kJ \cdot mol^{-1}$)
Acetamiprid		
20	25.07	16.90
40	24.94	17.33
60	25.32	17.91
Acetaminophen		
20	18.05	12.71
40	20.15	14.42
60	21.82	16.25

Declaration of Competing Interest

The authors declare that they have no known competing financial interests or personal relationships that could have appeared to influence the work reported in this paper.

Data availability

Data will be made available on request.

References

[1] G. Singh, K. Ramadass, P. Sooriyakumar, O. Hettithanthri, M. Vithange, N. Bolan, E. Tavakkoli, L. Van Zwieten, A. Vinu, Nanoporous materials for pesticide formulation and delivery in the agricultural sector, J. Control. Release 343 (2022) 187–206, https://doi.org/10.1016/j.jconrel.2022.01.036.
[2] R.S. Al-Farsi, M. Ahmed, A. Al-Busaidi, B.S. Choudri, Translocation of pharmaceuticals and personal care products (PPCPs) into plant tissues: A review, Emerg. Contam. 3 (2017) 132–137, https://doi.org/10.1016/j.emcon.2018.02.001.
[3] N. Le-Minh, S.J. Khan, J.E. Drewes, R.M. Stuetz, Fate of antibiotics during municipal water recycling treatment processes, Water Res. 44 (2010) 4295–4323, https://doi.org/10.1016/j.watres.2010.06.020.
[4] J. Haginaka, H. Sanbe, Uniform-sized molecularly imprinted polymers for 2-arylpropionic acid derivatives selectively modified with hydrophilic external layer and their applications to direct serum injection analysis, Anal. Chem. 72 (2000) 5206–5210, https://doi.org/10.1021/ac0005215.
[5] K. Farrington, F. Regan, Investigation of the nature of MIP recognition: The development and characterisation of a MIP for Ibuprofen, Biosens Bioelectron. 22 (2007) 1138–1146, https://doi.org/10.1016/j.bios.2006.06.025.
[6] A. Saravanan, P.S. Kumar, S. Jeevanantham, M. Anubha, S. Jayashree, Degradation of toxic agrochemicals and pharmaceutical pollutants: Effective and alternative approaches toward photocatalysis, Environ. Pollution. 298 (2022), 118844, https://doi.org/10.1016/j.envpol.2022.118844.
[7] B.M. Peake, R. Braund, A. Tong, L. Tremblay, The Life-Cycle of Pharmaceuticals in the Environment, Elsevier, 2015.
[8] U.S. McKnight, J.J. Rasmussen, B. Kronvang, P.J. Binning, P.L. Bjerg, Sources, occurrence and predicted aquatic impact of legacy and contemporary pesticides in streams, Environ. Pollution. 200 (2015) 64–76, https://doi.org/10.1016/j.envpol.2015.02.015.
[9] J.L. Tambosi, L.Y. Yamanaka, H.J. José, R.D.F.P.M. Moreira, H.F. Schröder, Recent research data on the removal of pharmaceuticals from sewage treatment plants (STP), Quím. Nova. 33 (2010) 411–420.
[10] K. Fent, A.A. Weston, D. Caminada, Ecotoxicology of human pharmaceuticals, Aquat. Toxicol. 76 (2006) 122–159, https://doi.org/10.1016/j.aquatox.2005.09.009.
[11] V.K. Gupta, A. Mittal, L. Kurup, J. Mittal, Adsorption of a hazardous dye, erythrosine, over hen feathers, J. Colloid Interface Sci. 304 (2006) 52–57, https://doi.org/10.1016/j.jcis.2006.08.032.
[12] V.K. Gupta, I. Ali, V.K. Saini, Adsorption studies on the removal of Vertigo Blue 49 and Orange DNA13 from aqueous solutions using carbon slurry developed from a waste material, J. Colloid Interface Sci. 315 (2007) 87–93, https://doi.org/10.1016/j.jcis.2007.06.063.
[13] V.K. Gupta, A. Mittal, V. Gajbe, J. Mittal, Removal and recovery of the hazardous azo dye acid orange 7 through adsorption over waste materials: Bottom ash and de-oiled soya, Ind. Eng. Chem. Res. 45 (2006) 1446–1453, https://doi.org/10.1021/ie051111f.

[14] V.K. Gupta, R. Jain, S. Malathi, A. Nayak, Adsorption–desorption studies of indigocarmine from industrial effluents by using deoiled mustard and its comparison with charcoal, J. Colloid Interface Sci. 348 (2010) 628–633, https://doi.org/10.1016/j.jcis.2010.04.085.
[15] V.K. Gupta, R. Jain, S. Varshney, Removal of Reactofix golden yellow 3 RFN from aqueous solution using wheat husk—An agricultural waste, J. Hazard Mater. 142 (2007) 443–448, https://doi.org/10.1016/j.jhazmat.2006.08.048.
[16] V.K. Gupta, I. Ali, Removal of endosulfan and methoxychlor from water on carbon slurry, Environ. Sci. Technol. 42 (2008) 766–770, https://doi.org/10.1021/es7025032.
[17] V.K. Gupta, B. Gupta, A. Rastogi, S. Agarwal, A. Nayak, Pesticides removal from wastewater by activated carbon prepared from waste rubber tire, Water Res. 45 (2011) 4047–4055, https://doi.org/10.1016/j.watres.2011.05.016.
[18] V.K. Gupta, A. Rastogi, Biosorption of lead from aqueous solutions by green algae Spirogyra species: Kinetics and equilibrium studies, J. Hazard Mater. 152 (2008) 407–414, https://doi.org/10.1016/j.jhazmat.2007.07.028.
[19] V.K. Gupta, A. Rastogi, A. Nayak, Biosorption of nickel onto treated alga (Oedogonium hatei): Application of isotherm and kinetic models, J. Colloid Interface Sci. 342 (2010) 533–539, https://doi.org/10.1016/j.jcis.2009.10.074.
[20] A.M. Redding, F.S. Cannon, S.A. Snyder, B.J. Vanderford, A QSAR-like analysis of the adsorption of endocrine disrupting compounds, pharmaceuticals, and personal care products on modified activated carbons, Water Res. 43 (2009) 3849–3861, https://doi.org/10.1016/j.watres.2009.05.026.
[21] J.L. Sotelo, G. Ovejero, A. Rodríguez, S. Álvarez, J. Galán, J. García, Competitive adsorption studies of caffeine and diclofenac aqueous solutions by activated carbon, Chem. Eng. J. 240 (2014) 443–453, https://doi.org/10.1016/j.cej.2013.11.094.
[22] J. Bedia, M. Peñas-Garzón, A. Gómez-Avilés, J.J. Rodriguez, C. Belver, A Review on the synthesis and characterization of biomass-derived carbons for adsorption of emerging contaminants from water, C. 4 (2018) 63, https://doi.org/10.3390/c4040063.
[23] S. Suresh, V. Viswanathan, M. Angamuthu, G.P. Dhakshinamoorthy, K.P. Gopinath, A. Bhatnagar, Lignin waste processing into solid, liquid, and gaseous fuels: a comprehensive review, Biomass Conv. Bioref. (2021), https://doi.org/10.1007/s13399-021-01497-8.
[24] J.J. Rodríguez, T. Cordero, J. Rodríguez-Mirasol, Carbon materials from lignin and their applications, in: Z. Fang, R.L. Smith (Eds.), Production of Biofuels and Chemicals From Lignin, Springer, Singapore, 2016, pp. 217–262, https://doi.org/10.1007/978-981-10-1965-4_8.
[25] J.M. Rosas, R. Ruiz-Rosas, J. Rodríguez-Mirasol, T. Cordero, Kinetic study of SO_2 removal over lignin-based activated carbon, Chem. Eng. J. 307 (2017) 707–721.
[26] L.M. Cotoruelo, M.D. Marqués, J. Rodríguez-Mirasol, J.J. Rodríguez, T. Cordero, Lignin-based activated carbons for adsorption of sodium dodecylbenzene sulfonate: Equilibrium and kinetic studies, J. Colloid Interface Sci. 332 (1) (2009) 39–45.
[27] J. Bedia, M. Peñas-Garzón, A. Gómez-Avilés, J.J. Rodriguez, C. Belver, Review on activated carbons by chemical activation with $FeCl_3$, C. 6 (2020) 21, https://doi.org/10.3390/c6020021.
[28] D.R. Lima, A. Hosseini-Bandegharaei, P.S. Thue, E.C. Lima, Y.R.T. de Albuquerque, G.S. dos Reis, C.S. Umpierres, S.L.P. Dias, H.N. Tran, Efficient acetaminophen removal from water and hospital effluents treatment by activated carbons derived from Brazil nutshells, Colloids Surf. A: Physicochem. Eng. Asp. 583 (2019), 123966, https://doi.org/10.1016/j.colsurfa.2019.123966.
[29] J. Żur, D. Wojcieszyńska, K. Hupert-Kocurek, A. Marchlewicz, U. Guzik, Paracetamol–toxicity and microbial utilization. Pseudomonas moorei KB4 as a case study for exploring degradation pathway, Chemosphere. 206 (2018) 192–202.
[30] R. Loos, D. Marinov, I. Sanseverino, D. Napierska, T. Lettieri, Review of the 1st watch list under the water framework directive and recommendations for the 2nd watch list, OP. (2018) 265.
[31] C.A. Morrissey, P. Mineau, J.H. Devries, F. Sanchez-Bayo, M. Liess, M.C. Cavallaro, K. Liber, Neonicotinoid contamination of global surface waters and associated risk to aquatic invertebrates: A review, Environ. Inter. 74 (2015) 291–303, https://doi.org/10.1016/j.envint.2014.10.024.
[32] S. Brunauer, P.H. Emmett, E. Teller, Adsorption of gases in multimolecular layers, ACS Publications. 60 (1938) 309–319.
[33] B.C. Lippens, B.G. Linsen, J.H. de Boer, Studies on pore systems in catalysts I. The adsorption of nitrogen; apparatus and calculation, J. Catalysis. 3 (1964) 32–37, https://doi.org/10.1016/0021-9517(64)90089-2.
[34] A. Gómez-Avilés, M. Peñas-Garzón, C. Belver, J.J. Rodriguez, J. Bedia, Equilibrium, kinetics and breakthrough curves of acetaminophen adsorption onto activated carbons from microwave-assisted $FeCl_3$-activation of lignin, Sep. Purif Technol. 278 (2021), 119654, https://doi.org/10.1016/j.seppur.2021.119654.
[35] M. Thommes, K. Kaneko, A.V. Neimark, J.P. Olivier, F. Rodriguez-Reinoso, J. Rouquerol, K.S. Sing, Physisorption of gases, with special reference to the evaluation of surface area and pore size distribution (IUPAC Technical Report), Pure. Appl. Chem. 87 (2015) 1051–1069.
[36] J. Bedia, C. Belver, S. Ponce, J. Rodriguez, J.J. Rodriguez, Adsorption of antipyrine by activated carbons from $FeCl_3$-activation of Tara gum, Chem. Eng. J. 333 (2018) 58–65, https://doi.org/10.1016/j.cej.2017.09.161.
[37] J.A. Menéndez, M.J. Illán-Gómez, C. Leon Y Leon, L. Radovic, On the difference between the isoelectric point and the point of zero charge of carbons 33 (1995) 1655–1657.
[38] H. Nourmoradi, K.F. Moghadam, A. Jafari, B. Kamarehie, Removal of acetaminophen and ibuprofen from aqueous solutions by activated carbon derived from Quercus Brantii (Oak) acorn as a low-cost biosorbent, J. Environ. Chem. Eng. 6 (2018) 6807–6815, https://doi.org/10.1016/j.jece.2018.10.047.
[39] D.T. Nguyen, H.N. Tran, R.-S. Juang, N.D. Dat, F. Tomul, A. Ivanets, S.H. Woo, A. Hosseini-Bandegharaei, V.P. Nguyen, H.-P. Chao, Adsorption process and mechanism of acetaminophen onto commercial activated carbon, J. Environ. Chem. Eng. 8 (2020) 104408.
[40] U. Zielke, K.J. Hüttinger, W.P. Hoffman, Surface-oxidized carbon fibers: I, Surface structure and chemistry, Carbon. 34 (1996) 983–998, https://doi.org/10.1016/0008-6223(96)00032-2.
[41] K. Qiu, X. Song, G. Tang, L. Wu, S. Min, Determination of fipronil in acetamiprid formulation by attenuated total reflectance-mid-infrared spectroscopy combined with partial least squares regression, Anal. Lett. 46 (2013) 2388–2399, https://doi.org/10.1080/00032719.2013.800537.
[42] F. Zapata, A. López-Fernández, F. Ortega-Ojeda, G. Quintanilla, C. García-Ruiz, G. Montalvo, Introducing ATR-FTIR spectroscopy through analysis of acetaminophen drugs: practical lessons for interdisciplinary and progressive learning for undergraduate students, J. Chem. Educ. 98 (2021) 2675–2686, https://doi.org/10.1021/acs.jchemed.0c01231.
[43] C.H. Giles, D. Smith, A. Huitson, A general treatment and classification of the solute adsorption isotherm. I. Theoretical, J. Colloid Interface Sci. 47 (1974) 755–765, https://doi.org/10.1016/0021-9797(74)90252-5.
[44] F. Dhaouadi, L. Sellaoui, B. Chavez-Gonzalez, H.E. Reynel-Ávila, L.L. Diaz-Muñoz, D.I. Mendoza-Castillo, A. Bonilla-Petriciolet, E.C. Lima, J.C. Tapia-Picazo, A. B. Lamine, Application of a heterogeneous physical model for the adsorption of Cd^{2+}, Ni^{2+}, Zn^{2+} and Cu^{2+} ions on flamboyant pods functionalized with citric acid, Chem. Eng. J. 417 (2021), 127975.
[45] F. Dhaouadi, L. Sellaoui, H.E. Reynel-Ávila, V. Landín-Sandoval, D.I. Mendoza-Castillo, J.E. Jaime-Leal, E.C. Lima, A. Bonilla-Petriciolet, A.B. Lamine, Adsorption mechanism of Zn^{2+}, Ni^{2+}, Cd^{2+}, and Cu^{2+} ions by carbon-based adsorbents: interpretation of the adsorption isotherms via physical modelling, Environ. Sci. Pollu, Research. 28 (2021) 30943–30954.
[46] L. Sellaoui, L.F. Silva, M. Badawi, J. Ali, N. Favarin, G.L. Dotto, A. Erto, Z. Chen, Adsorption of ketoprofen and 2-nitrophenol on activated carbon prepared from winery wastes: A combined experimental and theoretical study, J. Mole. Liq. 333 (2021), 115906.
[47] F.J. García-Mateos, R. Ruiz-Rosas, M.D. Marqués, L.M. Cotoruelo, J. Rodríguez-Mirasol, T. Cordero, Removal of paracetamol on biomass-derived activated carbon: Modeling the fixed bed breakthrough curves using batch adsorption experiments, Chem. Eng. J. 279 (2015) 18–30, https://doi.org/10.1016/j.cej.2015.04.144.
[48] A. Gómez-Avilés, L. Sellaoui, M. Badawi, A. Bonilla-Petriciolet, J. Bedia, C. Belver, Simultaneous adsorption of acetaminophen, diclofenac and tetracycline by organo-sepiolite: Experiments and statistical physics modelling, Chem. Eng. J. 404 (2021), 126601, https://doi.org/10.1016/j.cej.2020.126601.
[49] S.O. Akpotu, B. Moodley, Application of as-synthesised MCM-41 and MCM-41 wrapped with reduced graphene oxide/graphene oxide in the remediation of acetaminophen and aspirin from aqueous system, J. Environ. Manag. 209 (2018) 205–215, https://doi.org/10.1016/j.jenvman.2017.12.037.
[50] N.-A.-G. Nche, A. Bopda, D.R.T. Tchuifon, C.S. Ngakou, I.-H.-T. Kuete, A.S. Gabche, Removal of paracetamol from aqueous solution by adsorption onto activated carbon prepared from rice husk, J Chem Pharm Res. 9 (2017) 56–68.
[51] R.N. Coimbra, V. Calisto, C.I.A. Ferreira, V.I. Esteves, M. Otero, Removal of pharmaceuticals from municipal wastewater by adsorption onto pyrolyzed pulp mill sludge, Arab J. Chem. 12 (2019) 3611–3620, https://doi.org/10.1016/j.arabjc.2015.12.001.